ADVANCED MATERIALS

www.advmat.de

Efficient Flexible Solar Cell based on Composition-Tailored Hybrid Perovskite

*Cheng Bi, Bo Chen, Haotong Wei, Stephan DeLuca, and Jinsong Huang**

Organic–inorganic hybrid perovskites (OIHPs) are new photoactive layer candidates for lightweight and flexible solar cells due to their low-temperature process capability; however, the reported efficiency of flexible OIHP devices is far behind those achieved on rigid glass substrates. Here, it is revealed that the limiting factor is the different perovskite film deposition conditions required to form the same film morphology on flexible substrates. An optimized perovskite film composition needs a different precursor ratio, which is found to be essential for the formation of high-quality perovskite films with longer radiative carrier recombination lifetime, smaller density of trap states, reduced precursor residue, and uniform and pin-hole free films. A record efficiency of 18.1% is achieved for the flexible perovskite solar-cell devices made on an indium tin oxide/poly(ethylene terephthalate) substrate via a low temperature (≤100 °C) solution process.

Due to the compatibility to low-temperature solution process, organic–inorganic hybrid perovskites (OIHPs) are recognized as promising candidates of photoactive materials for light weight and flexible photovoltaic devices to fulfill the increasing needs from portable power source, such as unmanned systems, wearable electronics, consumer electronics, remote power, and automobiles.[1–7] During the past few years, the development of flexible OIHP solar cells has made significant progress in efficiency, bending durability, and specific weight (watts produced under AM1.5 1000 W m^{-2} irradiation to weight ratio), thanks to the high absorption coefficient, flexibility, and mechanical resilience of these materials.[1,4,5] The lightest flexible perovskite solar cells were demonstrated to have a record specific weight of 23 W g^{-1}, which raveled all other competing photovoltaic technology including copper indium gallium selenide, cadmium telluride (CdTe), organic photovoltaics (OPVs), and commercial large area module product of hydrogenated nanocrystalline silicon.[1,4,8,9] On the other hand, although the solution-processed OIHP thin film solar cells have been demonstrated very high power convert efficiency (PCE) of 22.1% on rigid substrates,[10,11] the most efficient OIHP solar cells were deposited on TiO_2 as electron transport layers (ETL) that requires a high temperature (≥450 °C) annealing.[12] This high temperature process is not comparable to the fabrication of flexible devices because the underneath polymer flexible substrates cannot sustain such a high temperature. This challenge has been partially solved by using compact TiO_2 ETL fabricated via magnetron sputtering or electron beam evaporation,[3] or using low-temperature-processed (≤150 °C) carrier transport materials, such as ZnO, poly(3,4-ethylenedioxythiophene)-poly(styrenesulfonate) and thiophene moieties (PhNa-1T), and solid-state ionic-liquids (1-benzyl-3-methylimidazolium chloride),[5–7,13] which improved the efficiency to 13.5%–16.1%.[7] However, these efficiencies are still far behind of those made on rigid substrates.

The challenge of fabrication high efficiency perovskite solar cells on flexible substrates remained to be a mystery, despite that the exactly same processes have been taken from those used on rigid substrates, and the conductivity of the flexible indium tin oxide (ITO) clearly is not a limiting factor in the small area devices. Here, we report that tuning the perovskite precursor ratio to tailor the composition of perovskite films on flexible ITO/poly(ethylene terephthalate) (PET) substrates is effective and crucial to improve their electronic properties and morphology, indicating a different precursor composition is need to achieve the same film morphology with that made on rigid ITO substrates. We demonstrated a record stabilized efficiency of 18.1% for flexible perovskite solar cells by improving the quality of perovskite films.

In this study, the flexible OIHP solar cells were fabricated on ITO-coated PET substrate with a planar heterojunction structure shown in **Figure 1**a. Poly(bis(4-phenyl)(2,4,6-trimethylphenyl)amine) (PTAA) and double fullerene layers (phenyl-C61-butyric acid methyl ester (PCBM) and C_{60}) were used as hole transport layer and ETL, respectively. Here, formamidinium (FA) cation was used to expand the absorption spectrum long edge of the perovskite films to 830 nm for an improved short-circuits current (J_{SC}). Methylammonium bromide (MABr, 10 wt%) was blended with formamidinium iodide (FAI) precursor solution to form mixed cation perovskite films for better thermal, moisture, and phase stability by modifying the tolerance factor.[14] For the perovskite solar cells made on rigid ITO/glass substrate with this composition, we obtained a high efficiency of 19.4% and 18.8% using the two-step

Dr. C. Bi, Dr. B. Chen, Dr. H. Wei, Prof. J. Huang
Department of Mechanical and Materials Engineering
and Nebraska Center for Materials and Nanoscience
University of Nebraska-Lincoln
Lincoln, NE 68588-0656, USA
E-mail: jhuang2@unl.edu
Dr. S. DeLuca
Energy Materials Corporation
Norcross, GA 30071, USA

DOI: 10.1002/adma.201605900

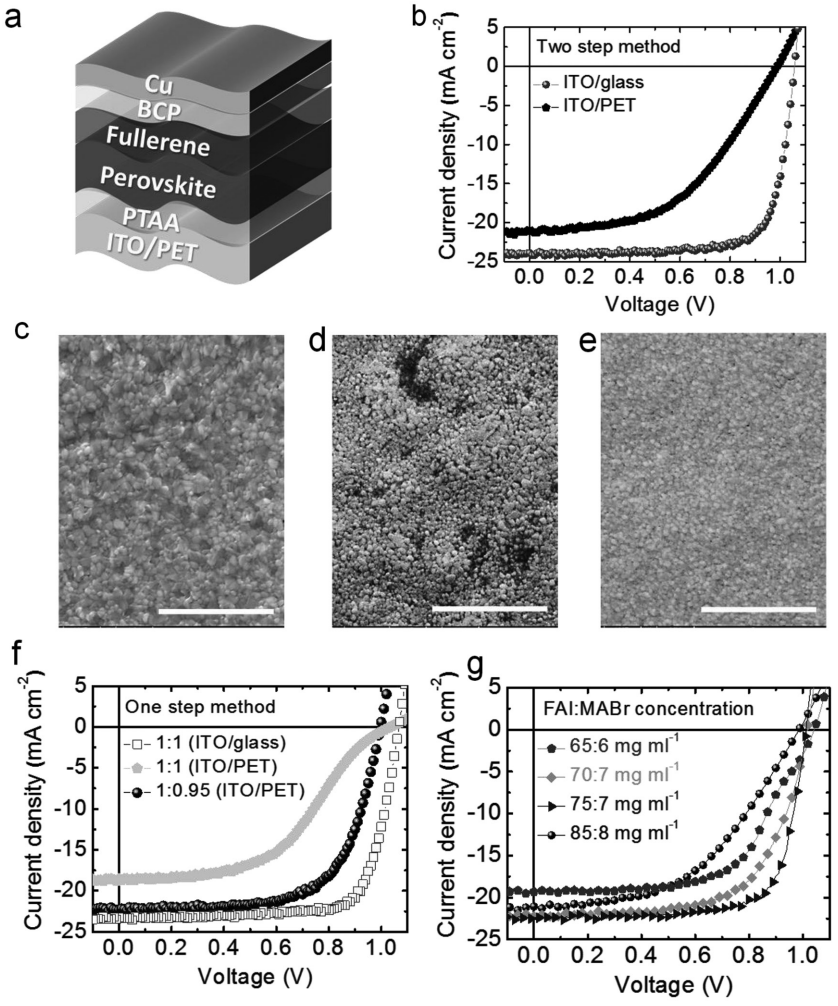

Figure 1. a) Scheme of flexible OIHP device structure. b) *J–V* measurement of the devices on ITO/glass and ITO/PET substrate with OIHP film grown by two-step interdiffusion method from a same deposition condition. scanning electron microscope (SEM) image of OIHP films on c) ITO/glass and d) ITO/PET substrate. The OIHP film deposition condition was same with that of devices shown in (b) (680 mg mL^{-1} PbI_2 and 85:8 mg mL^{-1} FAI:MABr solution). e) SEM image of the OIHP film on ITO/PET substrate with reduced FAI:MABr concentration of 75:7 mg mL^{-1}. Scale bars, 5 µm. f) *J–V* curve of the devices with one-step method grown OIHP films from a stoichiometric precursor (PbI_2: FAI = 1:1) on ITO/glass and ITO/PET substrate and nonstoichiometric precursor (PbI_2: FAI = 1:0.95) on ITO/PET substrate. g) *J–V* curve of the flexible devices with two-step interdiffusion grown OIHP films from varied FAI:MABr concentrations and a fixed PbI_2 thickness.

interdiffusion method and one-step antisolvent method to grow the perovskite films, respectively,[15,16] as shown in Figure 1b,f. Here, we used a stoichiometric molar ratio (1:1) of inorganic (PbI_2 and $PbBr_2$) and organic (FAI and MABr) precursors in one-step method. In striking contrast, the flexible device with the same deposition conditions had a significantly reduced efficiency of 9.0%, no matter the films were made by one-step or two-step deposition methods, as shown in Figure 1b,f. S-shape *J–V* curves were observed in almost all devices made with one-step method.

The difference of device performance should result from the different substrates because that was the only one changed. We initially speculated a thicker PTAA layer was formed on the ITO/PET substrate because of the observed S-shape *J–V* curve, which is usually caused by a large interface resistance. But this possibility was excluded because the devices still showed S-shape *J–V* curves and low fill factor (FF) even though the thinnest PTAA layers were deposited from diluted solutions, as shown in Figure S1 (Supporting Information). We then examined quality of perovskite films on ITO/PET substrate, which is one important factor to govern the device efficiency.[17,18] It has been demonstrated by us at early stage of perovskite research and many others that the film composition and morphology could be dramatically affected by precursor ratio used.[15,17,18] A slightly changed precursor ratio may significantly change the device efficiency, due to the formation of charge traps or defects at the grain boundary (GB) or surface that may damage carrier transfer/transport properties.[15,17,18] In this case, we speculate the composition and morphology of the perovskite films could be significantly affected by the different substrates used, despite that the precursor solutions applied were the same. To verify this speculation, we first examined the morphology of the perovskite films grown on both ITO/glass and ITO/PET substrates from a same deposition condition with two-step deposition method. We deposited the PbI_2 layers with a fixed thickness from a PbI_2 precursor solution with a concentration of 680 mg mL^{-1}, and we spun an organic precursor of FAI:MABr with a concentration of 85:8 mg mL^{-1}. It turned out the films on ITO/PET had worse topography with many pinholes on them, which was in strong contrast to the uniform films obtained on ITO/glass, as shown in Figure 1c,d. On the other hand, a reduced organic precursor concentration to 75:7 mg mL^{-1} yielded much uniform and smoother films on ITO/PET substrates, as shown in Figure 1e. Clearly, different substrates require different precursor ratio to reach the optimized morphology and composition of the perovskite films.

Since it is difficult to determine the composition of precursors that eventually formed the perovskite in two-step interdiffusion fabrication process, we did a composition tailoring with one-step film deposition method to highlight the needs of a changed composition for improved device performance on flexible substrates. We tailored the perovskite film composition made by one-step method by tuning the precursor ratio with a nonstoichiometric solution of PbI_2:FAI (1:0.95). The precursor solution still had a 10 mol% $MAPbBr_3$ to stabilize the FA-cation perovskite. The modified flexible solar cells had a more decent efficiency of 14.7% without showing an S-shape *J–V* curve, as displayed in Figure 1f. Then it is reasonable to deduce that

the excess FAI, rather than remaining PbI_2, which showed no trance in the X-ray diffraction (XRD) pattern in Figure S2 (Supporting Information), was responsible to the S-shape *J–V* curve in Figure 1f, because a reduced FAI amount in precursor solution eliminated the S-shape in the *J–V* curve. The excess FAI is likely on the surface of the grains or grain boundaries, which resulted in a thin insulating layer and thereby caused a low FF.[18] This result indicated the low efficiency actually came from the different quality of the perovskite films, or more specifically, different composition, and morphology on ITO/PET substrates. This result also confirms our very early discover that a stoichiometric precursor ratio does not necessarily guarantee a stoichiometric composition of the solid films, and an optimized recipe on one substrate is not guaranteed to be applicable on another one.[19] In this case, the difference of perovskite film quality should be caused by the different thickness, thermal conductivity, and the surface roughness (Figure S3, Supporting Information) of ITO/glass with respect to the flexible ITO/PET substrates.

To improve the device efficiency on flexible substrates, the perovskite film composition was optimized by tuning the precursor ratio in film deposition process by the two-step interdiffusion method. We focused two-step method to optimize the device efficiency because it has a better control of film thickness so that we can maximize the light absorption. We first deposited the PbI_2 layers with a fixed thickness from a PbI_2 precursor solution with a concentration of 680 mg mL^{-1}, and then the thickness of FAI:MABr precursor layer was optimized by changing the concentration of their solutions, while keeping all other deposition parameters unchanged. The *J–V* curve of the devices in Figure 1g showed a slight S-shape curve at lower FAI:MABr concentration of 65:6 mg mL^{-1}, probably due to incomplete reaction of PbI_2 with insufficient organic precursor.[15] An increased FAI:MABr concentration to 75:7 mg mL^{-1} improved the device FF and J_{SC} and resulted in a decent efficiency of 17.0%. An further increased FAI:MABr concentration of 85:8 mg mL^{-1}, though brought a PCE of 19.4% to the devices made on rigid ITO/glass substrates, reduced the efficiency to 10.1% for the flexible devices with a significantly smaller FF.

The gain size of the perovskite films on ITO/PET substrates was increased to further improve the efficiency because large grains are favorable in reducing total GB areas and thus total trap density.[20,21] One of our previous innovations to grow large perovskite grain is solvent annealing that facilitates GB migration by the solvent vapors, and dimethyl sulfoxide (DMSO) was one vapor that can increase the grain size of $MAPbI_3$,[21] though formation of complex with FA cation perovskite materials was also shown to tune the grain growth process and increase grain size.[14] Here, DMSO solvent annealing was found to significantly enlarge the grain size from 200–300 to 500–2000 nm, as shown in **Figure 2**a,b. Using DMSO solvent annealing, we obtained a higher PCE of 18.1%, with J_{SC} of 22.8 mA cm^{-2}, V_{OC} of 1.06 V, and FF of 74.6%, as shown in Figure 2c. The integrated J_{SC} from external quantum efficiency (EQE) in Figure 2d reached 21.9 mA cm^{-2}. On the other hand, the increase in J_{SC} is not significant. We measured stabilized photocurrent at maximum power output point to verify the measured efficiency. The stabilized photocurrent at the 0.85 V in Figure 2e was 21.3 mA cm^{-2} after 120 s under 1 Sun illumination, yielding an 18.1% stabilized efficiency. Most of the devices (64%) had PCE at the range of 14.0%–16.0%, as shown in the efficiency statistics from 25 devices at Figure 2f.

The change of film's optoelectronic properties upon varied precursor concentration was examined to find out the origin of the device PCE evolution shown above. Here, time-resolved photoluminescence (TRPL) measurement was performed to obtain the radiative carrier recombination lifetime of the films. The PL lifetime was extracted from PL decay curves in **Figure 3**a. It reveals that the optimized cation solution concentration of 75:7 mg mL^{-1} yielded a film with the longest PL lifetime of

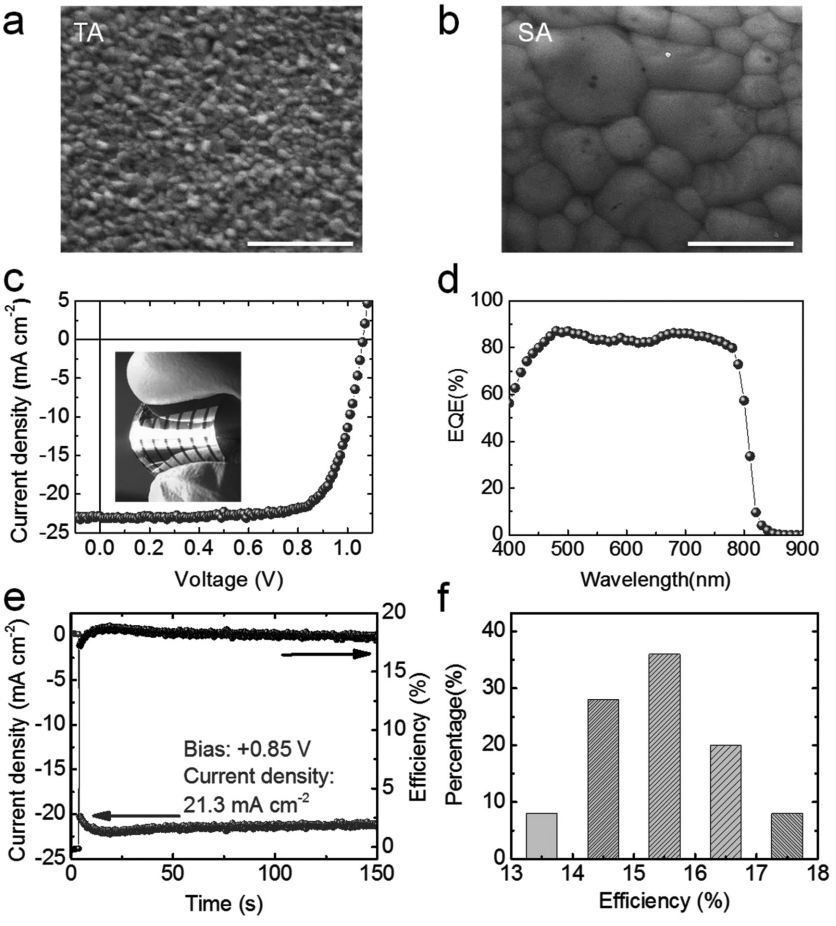

Figure 2. SEM images of the OIHP films grown by a) thermal annealing (TA) and b) DMSO solvent annealing (SA). Scale bar, 2 μm. c) *J–V* measurement. d) EQE and e) steady photocurrent at +0.85 V bias under 1 Sun illumination of the best-performing flexible OIHP device. f) Efficiency histogram of 25 flexible OIHP devices.

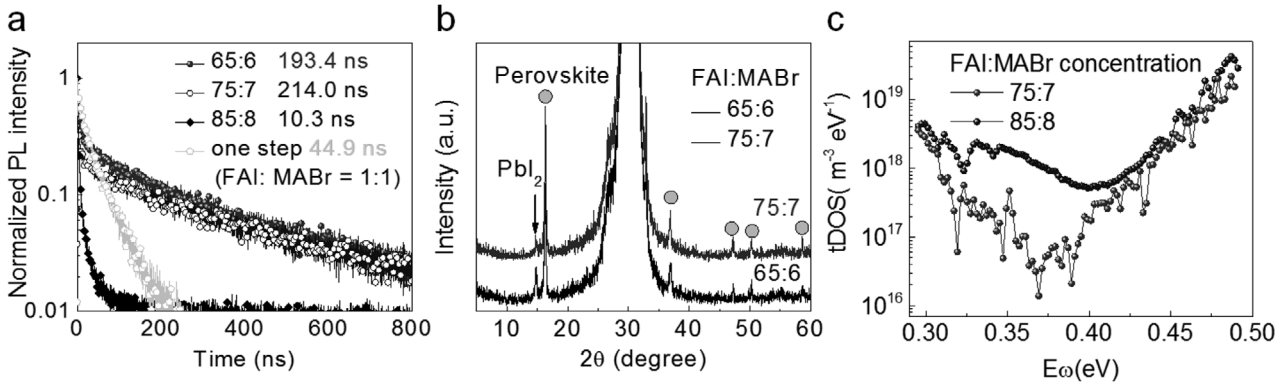

Figure 3. a) TRPL measurement on the OIHP films grown by two-step method from varied FAI:MABr concentrations and by one-step method from a stoichiometric precursor. b) XRD pattern of the OIHP films and c) tDOS of the OIHP devices with varied FAI:MABr concentrations.

214.0 ns. The long lifetime should be attributed to the suppressed nonradiative recombination from an optimized film composition. X-ray diffraction (XRD) measurement identified small trace of PbI_2 in the film, as shown in the Figure 3b. Certain amount of PbI_2 was proposed to passivate the OIHP film's GBs and to improve the carrier PL lifetime.[17,22] This explanation was further proven by the fact that the lower FAI:MABr concentration of 65:6 mg mL^{-1} that caused higher level of excess PbI_2 shown in Figure 3b had similar lifetime reaching 193.4 ns. Though too much PbI_2 residual may block carrier transfer at the interface and thereby result in inferior device efficiency, a little excess of PbI_2 does not necessarily quench the PL or to cause the nonradiative carrier recombination.[17,22,23] On the other hand, an excess FAI:MABr from 85:8 mg mL^{-1} solution significantly reduced the carrier lifetime by 20-fold to only 10.3 ns, possibly due to the strong quenching effect from the nonradiative recombination/deep trap states. The results revealed that the trap density can be strongly promoted by nonoptimized film composition from an overdose organic precursor, which eventually resulted in deteriorated device efficiency. The inferior perovskite films yielded larger trap density of states (tDOS) than optimized one by 0.5 to 1 order at the range of 0.30–0.42 eV, evidenced by thermal admittance spectroscopy (TAS) measurement shown in Figure 3c. The PL lifetime test also verified the composition dependent optoelectronic properties change of the perovskite films made by one-step method. The perovskite film from a mixed solution of 1:1 precursor ratio (PbI_2:FAI) was observed to have a shorter carrier lifetime to 44.9 ns, explaining the low device efficiency shown at Figure 1f. Reducing the organic precursor to the ratio of 1:0.95 (PbI_2:FAI) significantly improved the device efficiency shown at Figure 1f.

The device stability in the N_2 environment was evaluated. The devices showed only slight decrease in PCE from original 17.1% to 16.8% after two month of shelf lifetime testing, as shown in **Figure 4**a. The devices showed good stability because of the large grain size formed. In addition, the copper electrode in the devices was found to have no reaction with perovskite materials at room temperature for over 30 years.[1,24,25] While some broadly used metallic electrodes including Al and Ag required a diffusion barrier layer to reduced or slow down the reaction for better device stability.[1,25] The device's efficiency dropped to 16.2% after storage in N_2 for three months. The degraded device efficiency mainly suffered from a reduced FF from 75.0% to 69.8%, as shown in the inset of Figure 4a. We expect encapsulation of these devices would further improve the stability. One desired feature of flexible electronics to rigid ones is the mechanical flexibility under bending stress. We evaluated the flexible mechanical durability by bending at different bending curvature and bending cycles. First, we performed bending test with five curvature

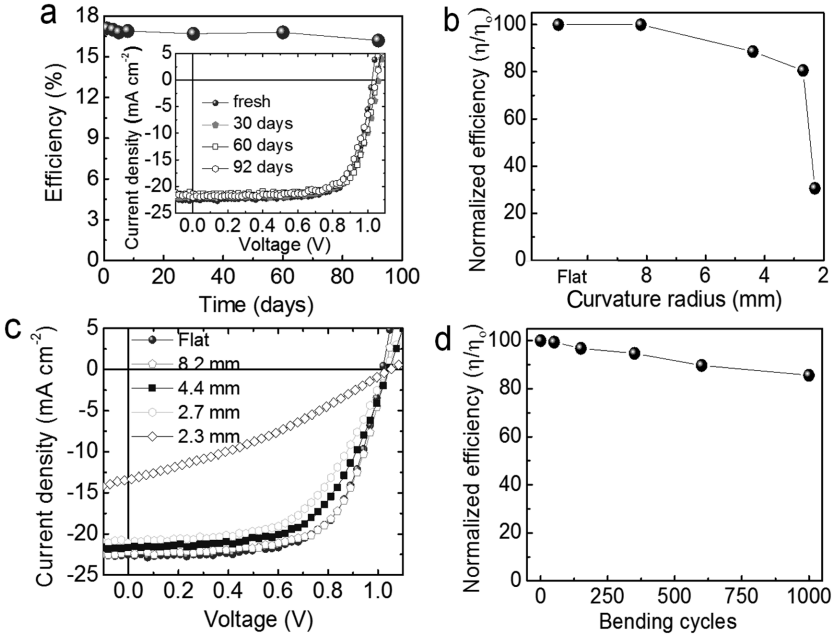

Figure 4. a) PCE and *J–V* curve (inset) evolution of the device stored in N_2 glove box. b) PCE and c) *J–V* curve evolution of the device upon increasing bending curvature radius. d) PCE evolution of the device upon increasing bending cycles at the bending curvature of 4.4 mm.

radii, from 8.2 to 2.3 mm under one bending cycle. The devices were measured after bending to find out the efficiency after bending. The Figure 4b shows the efficiency evolution upon varied bending curvature radii, and the inset shows the images of bending radii. The device PCE had almost no decrease after the bending with 8.2 mm curvature and then slightly decreased to 88.6% of original value at a curvature radius of 4.4 mm. The normalized PCE suffered obvious reduction to the 30.6% when curvature further lowered to 2.3 mm. The device FFs were observed to keep reducing upon decreased bending curvatures, as shown at Figure 4c. In the meanwhile, the series resistance increased by ten times from 5.4 to 58.8 Ω cm^2, most likely due to the generation of cracks in flexible ITO after bending.[26] A further bending caused the complete damage of the device. Next, we fixed the bending curvature to 4.4 mm and conducted bending test at multiple cycles. The device was found to keep 85.6% of its original efficiency after bending for 1000 cycles. The flexibility, defined by the curvature that causes the device failure and bending cycles, shown here is comparable to those reported flexible perovskite solar cells with an ITO/PET or ITO/polyethylene naphthalate (PEN) flexible substrate.[4,11,13,27] A further improvement on bending performance should look into the ITO layer that forms cracks under deformation. A potential solution is using highly conductive polymer layer with high mechanical brittleness to replace the broadly used conductive transparent metal-oxide electrode.[1,5,27]

In summary, we found the limitation to obtain efficient flexible perovskite solar cell was the inferior quality and composition of perovskite films, which was caused by the improper precursor ratio generally used. On the other hand, ITO/PET substrate required a different film deposition condition to ITO/glass substrate for an optimized composition in the film fabrication. The perovskite film composition was adjusted by tuning the precursor ratio to improve the film morphology and optoelectronic properties, which eventually improved the PCE to 18.1% on flexible ITO/PET substrate. Our findings here point out an important direction to develop high quality perovskite films on flexible substrates by tailored composition.

Experimental Section

ITO/PET Flexible Substrate Preparation: The ITO/PET flexible substrates were provided by Energy Materials Corporation. The substrates were etched by hydrochloric acid into half ITO-covered ones. A tap was used to cover part of ITO during hydrochloric acid etching. The etched substrates were cleaned by sonication in acetone.

Perovskite Film and Device Fabrication: FAI was synthesized and purified by the reported method.[14] In a typical fabrication process, the ITO/PET flexible substrates were spun with a PTAA layer from a 2 mg mL^{-1} solution in toluene at 6000 rpm. Then the as-prepared PTAA films were followed by a thermal annealing at 100 °C for 10 min. The mixed-cation OIHP films were deposited by thermal annealing-induced interdiffusion method and one-step antisolvent method.[15] First, 680 mg mL^{-1} PbI_2 precursor solution was prepared by dissolving PbI_2 (99.999% trace metals basis) in anhydrous dimethylformamide (DMF). Organic precursor solutions with different concentration and ratio were prepared by dissolving the FAI and MABr together in 2-propanol to form 65:6, 70:7, 75:7, and 85:8 mg mL^{-1} (FAI:MABr) solution. For one-step method, PbI_2, FAI, MABr, and $PbBr_2$ were dissolved together in a mixed solvent of DMF and DMSO (DMF:DMSO = 4:1 in volume ratio) to form a 1 M precursor solution. The MABr and $PbBr_2$ (1:1 molar ratio) had 10 mol% in total perovskite precursor solution. On the other hand, PbI_2 and FAI had varied molar ratio (PbI_2:FAI) from 1:0.95 and 1:1, respectively.

In two-step film fabrication method, the PbI_2 layer was deposited on top of PTAA by spin coating at 6000 rpm for 30 s from a preheated PbI_2 solution at 90 °C. The as-prepared PbI_2 film was dried at 90 °C for 5 min, and then it was followed by deposition of the 70 °C preheated FAI:MABr solution at 6000 rpm for 30 s. After that, the stacked precursor layers were dried at 70 °C for 15 min, and then it was followed by a thermal annealing at 100 °C for 60 min. In one step method, 60 µL of mixed perovskite precursor solution was first dropped on the PTAA-coated substrates, and then it started the spin coating. The spin rate was 2000 rpm for 10 s in the step one and then increased to 6000 rpm for 20 s in the step two. 120 µL of toluene was dropped onto the spinning film 5 s prior the end of the second step. The as-prepared films were then dried at 70 °C for 10 min and thermally annealed at 100 °C for 20 min. For solvent annealing, 2 µL DMSO was added in the edge of the Petri dish after the annealing temperature rose to 100 °C. All the film deposition and annealing processes were performed in an N_2-filled glove box.

To finish the device fabrication, a PCBM layer on top of the perovskite film was spun coat from a 20 mg mL^{-1} PCBM solution in dichlorobenzene at 6000 rpm for 30 s. A thermal annealing at 100 °C was applied to the PCBM layer for 45 min. Finally, it was sequentially deposited 20 nm C_{60}, 8 nm bathocuproine (BCP) layer, and 80 nm copper electrodes by vacuum thermal evaporation. The working area of the device is 10 mm^2.

Film Characterization: Perovskite films' surface morphology was studied by Quanta 200 FEG Environmental Scanning Electron Microscope. The perovskite films' XRD patterns were obtained by Rigaku D/Max-B X-ray diffractometer with Bragg–Brentano parafocusing geometry. A Co-Kα tube was employed with wavelength of 1.79 Å in emitted X-ray. TRPL of the perovskite films grown on flexible ITO/PET substrates was obtained in a Horiba DeltaPro fluorescence lifetime system. The excitation was provided by a DeltaDiode (DD-405) pulse laser diode with wavelength of 404 nm. The laser excitation energy was 2 pJ $pulse^{-1}$. The PL lifetime was obtained by fitting the PL decay curve with a biexponential decay:

$$I(t) = A_1 \exp\left(-\frac{t}{\tau_1}\right) + A_2 \exp\left(-\frac{t}{\tau_2}\right) \quad (1)$$

Here, the fast decay (decay time τ_1) was considered to the charge transfer from perovskite to PTAA layer, while the slow decay (decay time τ_2) resulted from radiative recombination. Then PL lifetime discussed in the paper is the time of slow decay (τ_2).

Device Characterization: The device's *J–V* curve was obtained under illumination of AM 1.5G irradiation (100 mW cm^{-2}), which was simulated by a Xenon-lamp-based solar simulator (Oriel 67005, 150 W Solar Simulator). Before photocurrent measurement, the light intensity was calibrated by an Si diode (Hamamatsu S1133) equipped with a Schott visible-color glass filter (KG5 color filter). The photocurrent was recorded by Keithley Model 2400 Source-Meter with a scanning rate of 0.07 V s^{-1}. EQE was obtained by a Newport QE measurement kit which focuses a monochromatic beam of light onto the devices working area. The bending test was performed in a home-made bending machine with a plier as holder.

The frequency-dependent capacitance (*C–f*) and voltage-dependent capacitance (*C–V*) were obtained by an *LCR* (inductance (*L*), capacitance (*C*), and resistance (*R*)) meter (Agilent E4980A). The devices' tDOS was derived from the obtained *C–f* and *C–V* in TAS measurement. The devices were under 1 Sun illumination at room temperature during the measurement of *C–f* and *C–V*. The derivation procedure can be found in ref. [28].

Supporting Information

Supporting Information is available from the Wiley Online Library or from the author.

Acknowledgements

This work was supported in part by Air Force Office of Scientific Research (AFOSR) (Grant No. A9550-16-1-0299) and Energy Material Corporation. J.H. has disclosed a significant financial interest in Energy Material Corporation.

Keywords

composition-tailored, flexible devices, low temperature solution process, perovskite solar cells

Received: November 1, 2016
Revised: January 10, 2017
Published online: June 9, 2017

[1] M. Kaltenbrunner, G. Adam, E. D. Głowacki, M. Drack, R. Schwödiauer, L. Leonat, D. H. Apaydin, H. Groiss, M. C. Scharber, M. S. White, *Nat. Mater.* **2015**, *14*, 1032.

[2] A. Chirilă, P. Reinhard, F. Pianezzi, P. Bloesch, A. R. Uhl, C. Fella, L. Kranz, D. Keller, C. Gretener, H. Hagendorfer, *Nat. Mater.* **2013**, *12*, 1107.

[3] a) W. Qiu, U. W. Paetzold, R. Gehlhaar, V. Smirnov, H.-G. Boyen, J. G. Tait, B. Conings, W. Zhang, C. B. Nielsen, I. McCulloch, *J. Mater. Chem. A* **2015**, *3*, 22824; b) D. Yang, R. Yang, J. Zhang, Z. Yang, S. F. Liu, C. Li, *Energy Environ. Sci.* **2015**, *8*, 3208.

[4] Y. Wang, S. Bai, L. Cheng, N. Wang, J. Wang, F. Gao, W. Huang, *Adv. Mater.* **2015**, *28*, 4532.

[5] Y. Li, L. Meng, Y. Yang, G. Xu, Z. Hong, Q. Chen, J. You, G. Li, Y. Li, *Nat. Commun.* **2016**, *7*, 10214.

[6] a) J. H. Heo, M. H. Lee, H. J. Han, B. R. Patil, J. S. Yu, S. H. Im, *J. Mater. Chem. A* **2016**, *4*, 1572; b) J. W. Jo, M. S. Seo, M. Park, J. Y. Kim, J. S. Park, I. K. Han, H. Ahn, J. W. Jung, B. H. Sohn, M. J. Ko, *Adv. Funct. Mater.* **2016**, *26*, 4464.

[7] D. Yang, R. Yang, X. Ren, X. Zhu, Z. Yang, C. Li, S. F. Liu, *Adv. Mater.* **2016**, *28*, 5206.

[8] A. Banerjee, F. S. Liu, D. Beglau, T. Su, G. Pietka, J. Yang, S. Guha, *IEEE J. Photovoltaics* **2012**, *2*, 104.

[9] A. Banerjee, T. Su, D. Beglau, G. Pietka, F. S. Liu, S. Almutawalli, J. Yang, S. Guha, *IEEE J. Photovoltaics* **2012**, *2*, 99.

[10] M. A. Green, K. Emery, Y. Hishikawa, W. Warta, E. D. Dunlop, *Prog. Photovoltaics Res. Appl.* **2016**, *24*, 905.

[11] J. You, Z. Hong, Y. M. Yang, Q. Chen, M. Cai, T.-B. Song, C.-C. Chen, S. Lu, Y. Liu, H. Zhou, *ACS Nano* **2014**, *8*, 1674.

[12] J. Burschka, N. Pellet, S.-J. Moon, R. Humphry-Baker, P. Gao, M. K. Nazeeruddin, M. Gratzel, *Nature* **2013**, *499*, 316.

[13] S. S. Shin, W. S. Yang, J. H. Noh, J. H. Suk, N. J. Jeon, J. H. Park, J. S. Kim, W. M. Seong, S. I. Seok, *Nat. Commun.* **2015**, *6*, 7410.

[14] W. S. Yang, J. H. Noh, N. J. Jeon, Y. C. Kim, S. Ryu, J. Seo, S. I. Seok, *Science* **2015**, *348*, 1234.

[15] Z. Xiao, C. Bi, Y. Shao, Q. Dong, Q. Wang, Y. Yuan, C. Wang, Y. Gao, J. Huang, *Energy Environ. Sci.* **2014**, *7*, 2619.

[16] M. Xiao, F. Huang, W. Huang, Y. Dkhissi, Y. Zhu, J. Etheridge, A. Gray-Weale, U. Bach, Y.-B. Cheng, L. Spiccia, *Angew. Chem., Int. Ed.* **2014**, *53*, 9898.

[17] D. Bi, W. Tress, M. I. Dar, P. Gao, J. Luo, C. Renevier, K. Schenk, A. Abate, F. Giordano, J.-P. Correa-Baena, J.-D. Decoppet, S. M. Zakeeruddin, M. K. Nazeeruddin, M. Grätzel, A. Hagfeldt, *Sci. Adv.* **2016**, *2*, e1501170.

[18] D.-Y. Son, J.-W. Lee, Y. J. Choi, I.-H. Jang, S. Lee, P. J. Yoo, H. Shin, N. Ahn, M. Choi, D. Kim, N.-G. Park, *Nat. Energy* **2016**, *1*, 16081.

[19] Q. Wang, Y. Shao, Q. Dong, Z. Xiao, Y. Yuan, J. Huang, *Energy Environ. Sci.* **2014**, *7*, 2359.

[20] C. Bi, Q. Wang, Y. Shao, Y. Yuan, Z. Xiao, J. Huang, *Nat. Commun.* **2015**, *6*, 7747.

[21] Z. Xiao, Q. Dong, C. Bi, Y. Shao, Y. Yuan, J. Huang, *Adv. Mater.* **2014**, *26*, 6503.

[22] Q. Chen, H. Zhou, T.-B. Song, S. Luo, Z. Hong, H.-S. Duan, L. Dou, Y. Liu, Y. Yang, *Nano Lett.* **2014**, *14*, 4158.

[23] Y. H. Lee, J. Luo, M.-K. Son, P. Gao, K. T. Cho, J. Seo, S. M. Zakeeruddin, M. Grätzel, M. K. Nazeeruddin, *Adv. Mater.* **2016**, *28*, 3966.

[24] a) Y. Deng, Q. Dong, C. Bi, Y. Yuan, J. Huang, *Adv. Energy Mater.* **2016**, *6*, 1600372; b) J. Zhao, X. Zheng, Y. Deng, T. Li, Y. Shao, A. Grouverman, J. E. Shield, J. Huang, *Energy Environ. Sci.* **2016**, *9*, 3650.

[25] K. Domanski, J.-P. Correa-Baena, N. Mine, M. K. Nazeeruddin, A. Abate, M. Saliba, W. Tress, A. Hagfeldt, M. Grätzel, *ACS Nano* **2016**, *10*, 6306.

[26] Y. Yuan, Y. Bi, J. Huang, *Appl. Phys. Lett.* **2011**, *98*, 063306.

[27] K. Poorkazem, D. Liu, T. L. Kelly, *J. Mater. Chem. A* **2015**, *3*, 9241.

[28] a) Y. Shao, Z. Xiao, C. Bi, Y. Yuan, J. Huang, *Nat. Commun.* **2014**, *5*, 5784; b) C. Bi, Y. Yuan, Y. Fang, J. Huang, *Adv. Energy Mater.* **2015**, *5*, 1401616.

